Journal of ELECTRONIC MATERIALS, Vol. 50, No. 4, 2021
https://doi.org/10.1007/s11664-021-08766-2
© 2021 The Minerals, Metals & Materials Society

ORIGINAL RESEARCH ARTICLE

Solution-Processable $LaTiO_x$-PVP as Silicon-Free Gate Dielectric at Low Temperature for High-Performance Organic-Inorganic Field Effect Transistors

HAMED NAJAFI-ASHTIANI,[1,5,6] ALIREZA TAVOUSI,[2] ALI RAMZANNEZHAD,[3] and ABBAS RAHDAR[4]

1.—Department of Physics, Faculty of Science, Velayat University, P.O. Box 99111-31311, Iranshahr, Iran. 2.—Department of Electrical Engineering, Velayat University, P.O. Box 99111-31311, Iranshahr, Iran. 3.—Department of Solid-State Physics, University of Mazandaran, Babolsar, Iran. 4.—Department of Physics, University of Zabol, Zabol, Iran. 5.—e-mail: h.najafi@velayat.ac.ir. 6.—e-mail: hamednajafi59@yahoo.com

We report that the organic-inorganic composite of polyvinyl phenol (PVP) and lanthanum titanate can be used as a gate dielectric layer of a low-voltage thin film transistor (TFT). The high-k organic-inorganic composite is synthesized at low temperatures through a solution-processable method and deposited by a simple spin-coating technology on polyethylene terephthalate coated by indium tin oxide (PET-ITO) film substrate. The fabricated devices show small and positive threshold voltage, and thus are applicable for low-power and high-speed operation. Thin film organic-inorganic composite transistors show high current on/off on order of 10^4, dependent on composition. Organic-inorganic thin film transistors (TFTs) fabricated using composite of polyvinyl phenol and lanthanum titanate layers as gate dielectric and zinc oxide (ZnO) films as channel layers exhibit superior electron transport characteristics with the electron mobility of 1.04 $cm^2\ V^{-1}\ s^{-1}$, while the ratio of channel width (W) to channel length (L) for these devices is 20.

Key words: Solution process, lanthanum titanate, field-effect transistor, silicon-free gate electrode, low temperature

INTRODUCTION

Organic-inorganic thin film transistors (TFTs) are a promising technology for a wide range of electronic applications such as system-on-glass displays, flat-panel displays, organic light-emitting diode displays (OLED) and liquid crystal screens.[1–3] The production process of organic-inorganic TFTs must have low cost, low temperature and the potential for appropriate-area solution-processable fabrication. Despite their relatively short history, organic-inorganic TFTs based on a silicon-free gate dielectric have already demonstrated acceptable performance that is comparable to that of a silicon-based gate dielectric as conventional field-effect transistors (FETs).[4,5] Whilst progress in the field of semiconducting post-transition metal oxides (ZnO, ZrO_2, In_2O_3, Al_2O_3, HfO_2, InZnO, InGaZnO, etc.) has been rapidly advancing, research efforts have been focused on the development of new fabrication technologies for these oxide TFTs.[6–18]

Although we can mention another group of functional oxide materials with excellent electrical properties called ferrites, the importance of their dielectric properties, which depends on their magnetic contribution, cannot be ignored.[19,20] For these purposes, it is more profitable to use not just the dielectrics, but the magneto-dielectrics.

Despite the wide energy bandgaps and suitable electrical properties of the transition metal oxides (TMO), the utilization of higher fabrication temperatures for producing, processing and device improvement can

(Received April 21, 2020; accepted January 18, 2021; published online February 10, 2021)

prevent the use of flexible substrates and organic materials.[21] Although there are various methods for synthesizing precursor oxide nanoparticles,[22–24] in order to not be deprived of the benefits of flexible substrates, optical transparency and organic materials, low-temperature fabrication based on a solution-processable method is needed.[7,9,25,26] Nevertheless, the development of new solution-processable gate dielectric layers has been neglected in the domain of metal oxide TFTs. That is because in low-cost deposition techniques such as spin-coating, post-annealing (> 300 °C) is an important and powerful tool to overcome unwanted impurities, such as peripheral carbon, hydroxyl groups and oxygen vacancies, which lead to performance enhancement of TMO high-k gate dielectric films through modifying leakage current and capacitance characteristics.[27] Today, organic-inorganic composites have shown various practical advantages in the applied industries, which can generally be referred to as polymer-ceramic composites and polymer-metal oxide composites.[28–33] One possible way to overcome such problems is utilization of organic materials as an alternative gate dielectric based on properties including low cost, low temperature, high flexibility and reduced leakage current. But thin layers of organic gate dielectric (less than several hundred nanometers) in TFTs suffer from numerous pinholes and defects that subsequently result in surface roughness and poor dielectric strength.[34,35] Typically, a thick layer of organic gate dielectric decreases the capacitance density of the gate dielectric that enables a high-voltage device to be achieved.[36] However, various organic dielectrics have been investigated, including polyimide (k = 2.5), polystyrene (k = 2.6), benzocyclobutene (k = 2.7), parylene (k = 2.7), polymethylmethacrylate (k = 3.5), polyvinyl chloride (k = 4.6), polyvinyl phenol (k = 5) and polyvinyl alcohol (k = 7.8) as interesting organic gate dielectrics in organic field-effect transistors (OFETs).[37,38] Therefore, apart from the benefits of organic materials, they typically have relatively low k values, and thus at low operating voltages, drain-source current exhibits frequently insufficient current.[39] On the other hand, utilization of high-k metal oxide layers typically requires high post-annealing temperatures (> 400 °C) to ensure reasonable low leakage currents that limits use of flexible substrates. Recently, the hybrid or composite of organic-inorganic gate dielectric films were introduced as a reliable nominate gate dielectric for high-performance and low-temperature organic inorganic TFTs.[2,37,38,40]

In this work, it is shown that the low-temperature-synthesized organic-inorganic composite based on lanthanum titanite as inorganic high-k dielectric and polyvinyl phenol (PVP) as organic high-k dielectric is a good candidate for silicon-free gate dielectric in TFTs. The benefits of using fabricated thin film transistors based on lanthanum titanite-PVP gate dielectric are thoroughly shown by electrical characterization. The positive and low threshold voltage, current on/off on order of 10^4 and acceptable output current of the source to drain along with the low-temperature features of the synthesis and simple deposition technique are the advantages of this device.

EXPERIMENTAL

Materials

Lanthanum nitrate hexahydrate ($La(NO_3)_3{\cdot}6H_2O$, Aldrich), titanium chloride ($TiCl_4$, Aldrich), 3-(trimethoxysilyl) propyl methacrylate (silane, 98%) and poly(4-vinylphenol) (PVP) were procured from Sigma-Aldrich and Alfa-Aesar. All solvents, including ethanol (EtOH, 99.99%), deionized water and nitric acid were purchased from Merck. The polyethylene terephthalate coated by indium tin oxide (PET-ITO) film (sheet resistance < 6 Ω/□) was obtained from Xinyan Technology Ltd. and used as flexible gate electrode. The sputtering targets with high purity (> 99.99%, American Elements), 75.6 mm diameter and 6.35 mm thickness were used for deposition of the zinc oxide (ZnO) channel and indium tin oxide (ITO) source and drain electrodes.

Dielectric Film Preparation

An initial precursor solution for the inorganic contribution of gate dielectric ($LaTiO_x$) was formulated by dissolving titanium chloride ($TiCl_4$, Aldrich) and lanthanum nitrate hexahydrate ($La(NO_3)_3{\cdot}6H_2O$, Aldrich) in ethanol with the same molar ratio of La/Ti, which was then stirred continuously for 5 h at 60°C until titanium chloride and lanthanum nitrate had dissolved completely and produced a uniform solution with the concentration of 0.1 M. The nitric acid and H_2O (1 M) were added as an oxidant and silane as a coupling agent into the $LaTiO_x$ precursor solution at room temperature and under gentle stirring for 1 h. In order to provide an organic material contribution solution for gate dielectric composite, ethanol as solvent was used to dissolve PVP as organic dielectric by continuous stirring for 1 h. The prepared organic and inorganic solutions were combined and stirred to complete hydrolysis and condensation proceeding at 70 °C with the various ratios of PVP solution (presented in Table I) to obtain dilute, homogeneous and stable gel. Figure 1a shows a schematic of the synthesis process. The $LaTiO_x$-PVP (LTOP) gate dielectric layers were deposited by spin-coating technique on the silicon-free PET-ITO substrate at 5000 rpm for 20 s, followed by drying at room temperature for 12 h to eliminate the solvent.

Material Characterization Techniques

Thermogravimetric Analysis (TGA)

The thermal response of synthesized $LaTiO_x$-PVP composite was examined by thermogravimetric analysis (TGA) using an STA 504 thermal analyzer

Table I. The material weight ratios to obtain organic-inorganic composites.

Sample	Titanium chloride	Lanthanum nitrate hexahydrate	PVP	Silane
LTOP1	1	0.33	0.5	0.1
LTOP2	1	0.33	1.0	0.1
LTOP3	1	0.33	1.5	0.1

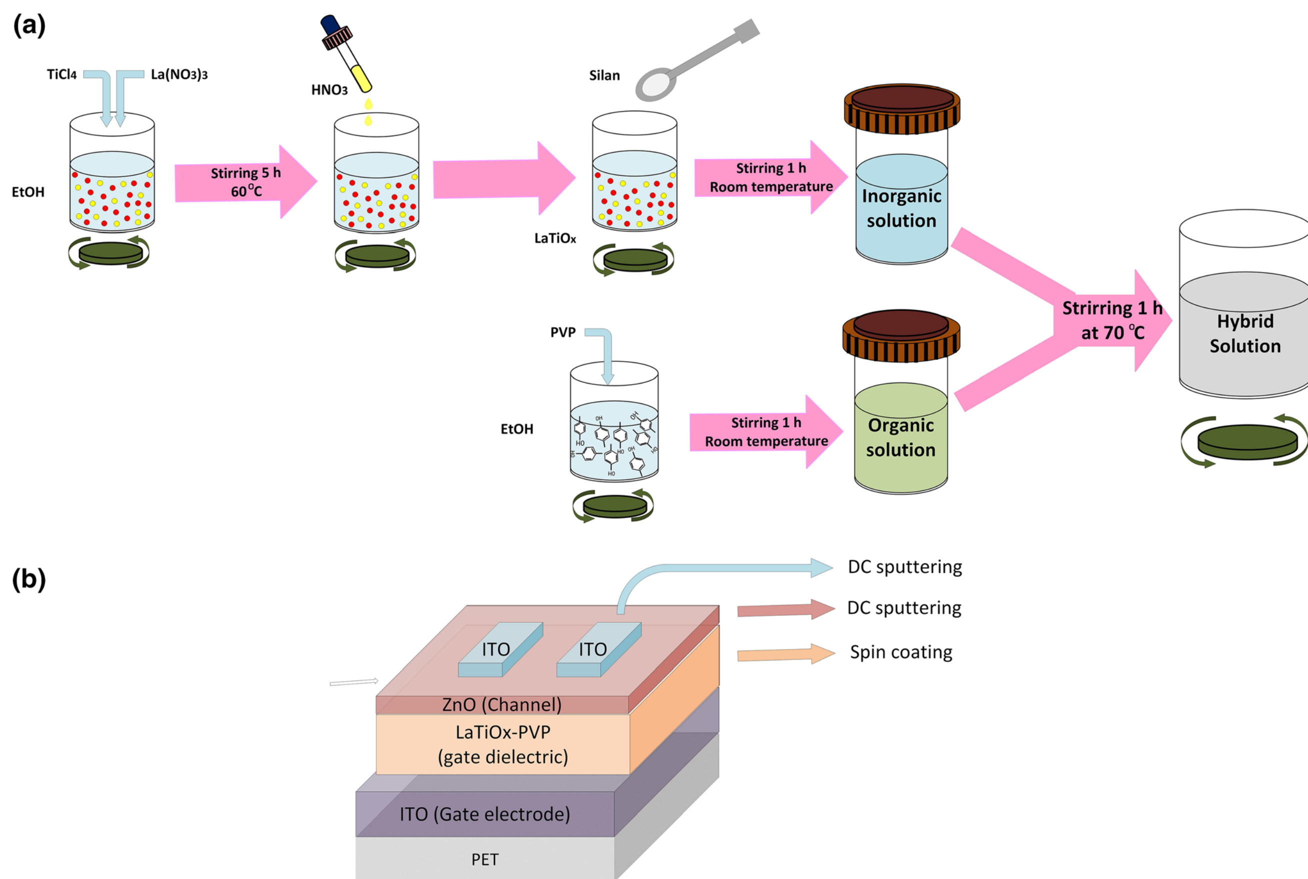

Fig. 1. (a) Schematic of LaTiOx-PVP composite synthesis. (b) Schematic diagram of the thin film transistors (TFTs) in bottom-gate/top-contact/PET-substrate configuration based on silicon-free substrate.

at a heating rate of 283 K per min in air atmosphere.

X-ray Diffraction

The structural properties of the $LaTiO_x$-PVP composite were characterized by using a GBC MMA x-ray diffractometer with Cu-Ka radiation (λ = 1.54056 Å) operated at 35 kV in the 2θ range of 5°–70° with a step of 0.04°.

Fourier Transform Infrared Spectroscopy (FTIR)

The chemical functional groups of $LaTiO_x$-PVP composite coatings were identified using Fourier transform infrared spectroscopy (FTIR) (Bruker, Tensor 27) in the range of 400–4000 cm^{-1}.

X-ray Photoelectron Spectroscopy

The chemical properties of $LaTiO_x$-PVP composite gate dielectric layers were evaluated by x-ray photoelectron spectroscopy (XPS) using a Thermo Scientific K-Alpha spectrometer with an Al Ka source (1486.7 eV) operated at a power of 200 W (10 kV and 20 mA). The binding energy estimates were calibrated by fixing the C1*s* peak with a binding energy of 285 eV.

Atomic Force Microscopy (AFM)

The surface morphology of the $LaTiO_x$-PVP composite gate dielectric coatings was investigated by atomic force microscopy (AFM; AutoProbe, CP Research, Veeco).

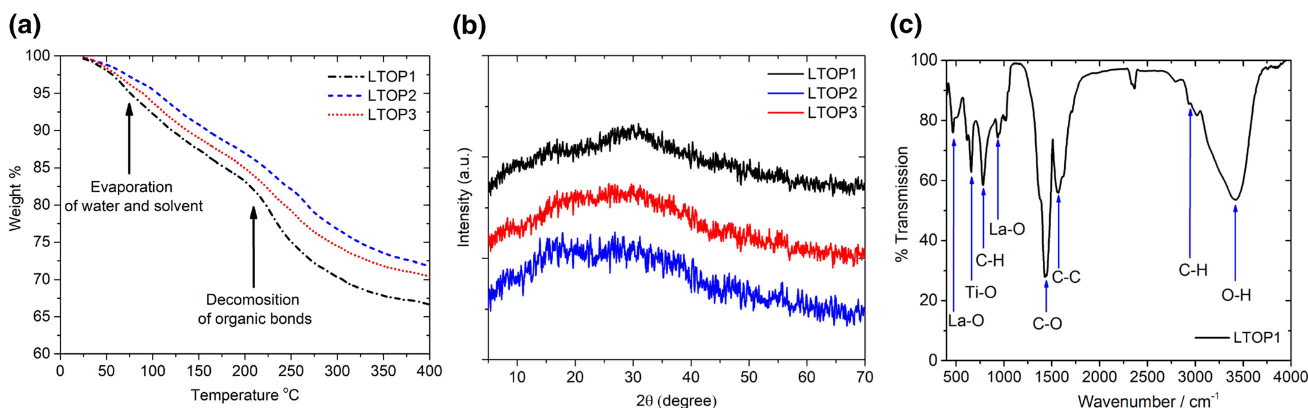

Fig. 2. (a) TGA spectra of organic-inorganic composites for an organic-inorganic composite gate dielectric with different ratios of organic materials as a function of temperature in a range from 25 °C to 400 °C. (b) XRD patterns of organic-inorganic composites for the lanthanum titanite-PVP (LTOP) structures with different ratios of PVP. (c) FTIR spectrum of the synthesized organic-inorganic composite (LTOP1) in the range of 400–4000 cm^{-1}.

Capacitance–Voltage and Current–Voltage Characterization

The capacitance–voltage (C–V) was evaluated due to the capacitor structure by using an HP 4284A analyzer at frequencies in the 1 kHz to 1 MHz range, and the current–voltage (I–V) curves were obtained using a Keithley 4200 semiconductor analyzer.

Device Fabrication

The ZnO layer was coated as a transistor channel with thickness of 50 nm on the LaTiO$_x$-PVP composite gate dielectric substrates by direct-current (DC) magnetron sputtering in an argon atmosphere. The sputtering parameters such as working pressure and DC power were 0.32 Pa and 90 W, respectively, during the deposition of ZnO layer. The ITO pads as source and drain electrodes were coated on the ZnO layer by DC sputtering technique and usage of a shadow mask with a working pressure of 0.67 Pa, argon flow rate of 15 sccm and DC power of 50 W. Figure 1b shows the schematic diagram of fabricated thin film transistors.

RESULTS AND DISCUSSION

Structural and Morphological Studies

Thermogravimetric analysis (TGA) was carried out to estimate the effects of temperature on the stability of the organic inorganic gate dielectric structure. The consumption of power in electronic devices results in an increases of device temperature, while the only way to cool the device is by a thermal transmission process through the peripheral environment. Thus, the thermal decomposition behavior of organic inorganic gate dielectrics, shown in Fig. 2a, is an important parameter. The curve behavior exhibits two steps of weight loss as a function of temperature in the range of 25 °C to 400 °C, and by increasing the organic material in structures, the weight loss process increases. For these structures, evaporation of water and solvent occurs in the range of 65 °C to 85 °C, while the decomposition of organic bonds occurs between 180 °C and 225 °C. Therefore, the temperature tolerance threshold of these structures is as high as 180 °C.

The chemical synthesized metal oxides have an amorphous structure, and by the post-annealing process, they exhibit microcrystal structures. Figure 2b shows the XRD characterization of organic inorganic gate dielectric films deposited on Si wafer substrate by spin-coating technique in the range of 2q from 5° to 70°. The x-ray diffraction data exhibit broad amorphous-like features located at around $2\theta = 30°$, which is in accordance with the low-temperature synthesis process. In order to show the chemical functional groups of the organic–inorganic composite gate dielectric (LTOP1 sample), the FTIR spectrum is presented in Fig. 2c. The spectrum is measured in the wavelength range of 400–4000 cm^{-1}. The transmission peaks at 3427 and 2923 cm^{-1} correspond to the stretching vibration of the O–H bond and the stretching vibration of the C–H bond. The peaks appearing at 1578, 1438, 834 and 797 cm^{-1} are assigned to the stretching vibrations of the C–C bond of the quoined, the vibration modes of the C–O bond, the vibration modes of the C–H bond and the stretching of the C–H bond for para-substituted aromatic rings, respectively. Additionally, the peaks observed at 1020, 655 and 467 cm^{-1} are related to the stretching vibration of the La–O bond, Ti–O bond and the La–O bond.

In order to evaluate the stoichiometry and chemical composition of lanthanum titanite film (LTO), we employed x-ray photoelectron spectroscopy (XPS). Figure 3a shows the survey XPS spectrum for LTO film deposited on Si wafer substrate by spin-coating technique. All the spectra are correlated with the C1s peak located at 285.0 eV. The stoichiometry of LaTiO$_x$ can be evaluated by the XPS survey spectrum. The lanthanum and titanium

atomic concentrations are 11.1% and 11.1%, respectively, while the oxygen concentration is 66.0%. These percentage concentrations show that the stoichiometry of synthesized lanthanum titanate with x = 2.97 ± 0.05 is $LaTiO_{2.97}$. It is well known that the complex ceramic samples easily allow the oxygen excess or deficit.[41–43] Furthermore, oxygen excess and deficit can change electrical parameters such as the DC and AC resistivity and bandgap. An increase in the unit cell parameter may be also due to oxygen deficiency. XPS high-resolution spectra introduce a higher signal-to-noise ratio compared to survey scans and are therefore reasonable for the estimation of minor changes in surfaces chemistry that are not observable in survey spectra. Figure 3b, c and d show the high-resolution XPS La 3d, Ti 2p and O 1s spectra for the LTO film. The La 3d is two doublets because of the spin-orbit splitting of La $3d_{5/2}$ and La $3d_{3/2}$ with a separation energy of 17 eV, while each doublet is split with a separation energy of 4.4 eV due to a transfer of an electron from O 2p to the empty La 4f shell leading to the $3d^9\ 4f^1$ final state (Fig. 3b).[44] The convoluted-high resolution XPS spectrum of the Ti 2p orbital is shown in Fig. 3c. The Ti 2p is a doublet because of the spin-orbit splitting of Ti $2p_{3/2}$ (located at 459.5 eV) and Ti $2p_{1/2}$ (located at 465.4 eV) with a separation energy of 5.9 eV.[2] The asymmetric O 1s peak (Fig. 3d) can also be fitted into 531.3 and 532.5 eV. The main lattice peak (located at 531.3 eV) of O 1s is consistent with the typical O 1s peak position of stoichiometric La_2O_3 or TiO_2, while the peak at 532.5 eV is attributed to the oxygen deficiency lattice peak.[27,45]

The transistor efficiency based on the charge carrier transport, dielectric constant and contact resistance in organic-inorganic gate dielectric strongly depends on the interface between the gate dielectric and semiconductor layers.[1,3,11,46]

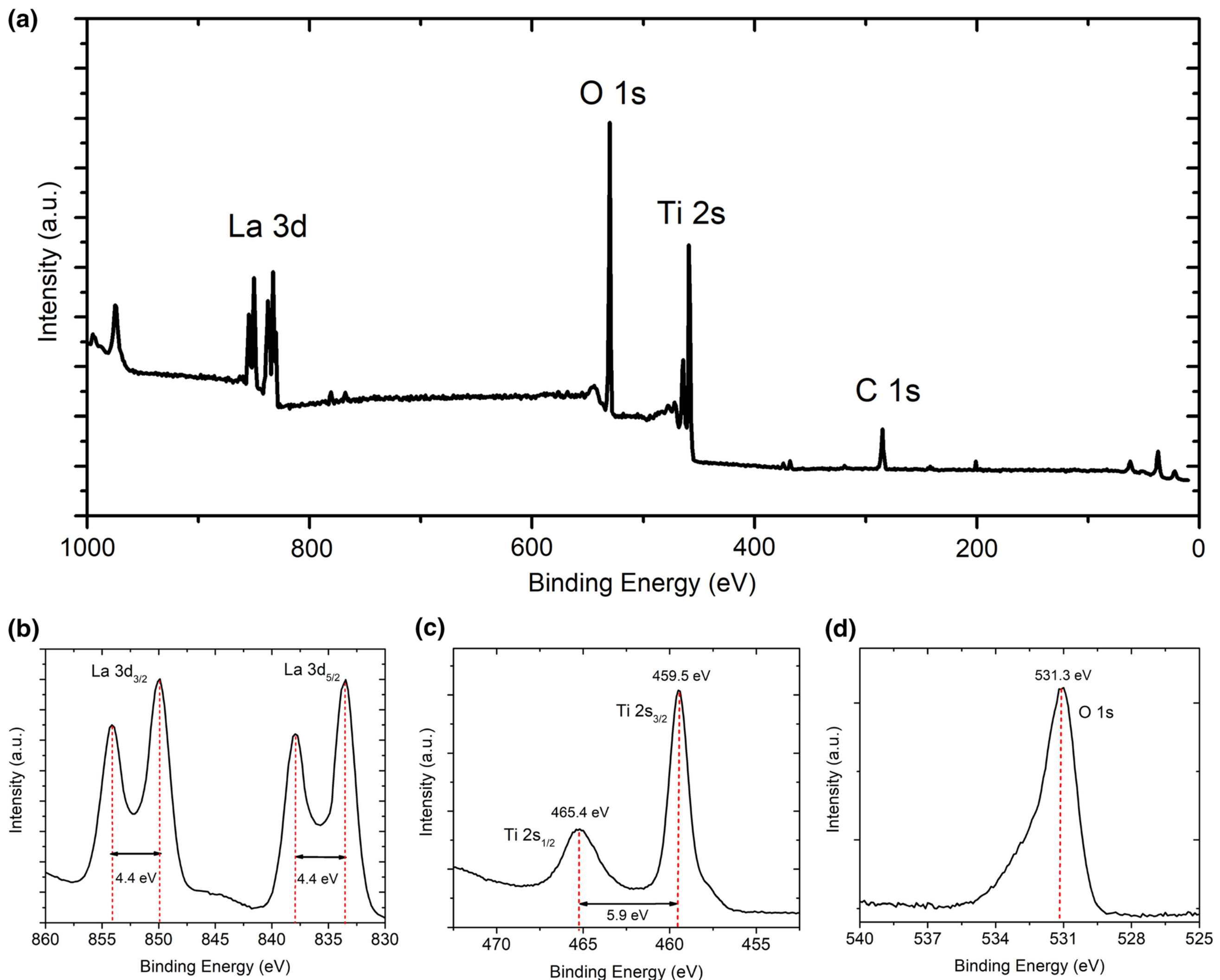

Fig. 3. XPS surface chemistry characterization of LTOP composite. (a) XPS survey spectrum of LTOP composite. (b) High-resolution XPS spectrum of La 3d. The La 3d is two doublets based on the spin-orbit splitting of La $3d_{5/2}$ and La $3d_{3/2}$ with a separation energy of 17 eV. (c) High-resolution XPS spectrum of Ti 2p. The Ti 2p is a doublet because of the spin-orbit splitting of Ti $2p_{3/2}$ and Ti $2p_{1/2}$ with a separation energy of 5.9 eV. (d) High-resolution XPS spectrum of O 1s.

Therefore, the device performance depends on the properties of these interfaces. To evaluate this property, the surface morphology and roughness are examined by AFM, and the scanned areas of samples and their data are show in Fig. 4. Figure 4a, b and c shows the tapping-mode AFM images of LTOP1, LTOP2 and LTOP3 coatings, respectively, with their histogram curves due to the Gaussian form with the least breadth. As seen, no surface defects and pinholes are observed, which confirms the high quality of the solution-processed film fabricated by spin-coating technique. The size of the crystallites influences the properties of the crystal structure, and therefore the electrical properties are affected by the average grain size of the composites. Mass transport, and especially oxygen vacancies transport, destroys the grains in a crystalline structure, and a decrease in the grain size reduces the unit cell volume, which can be explained by an increase in the surface tension compared to elastic forces in the bulk material.[47,48]

Electrical Characteristics of Gate Dielectrics

To demonstrate the performance of our organic-inorganic composite gate dielectric system, bottom-gate, top-contact LTOP FETs with ITO source-drain electrodes are arranged using the thin film structure. Three organic-inorganic composite gate dielectrics (LTOPs) based on ITO substrates as gate are used and tested. ITO source and drain electrodes are deposited by using a shadow mask with dimensions of L (channel length) = 100 μm and W (channel width) = 2000 μm. In mobile communication systems, dielectric materials constitute an important part of radio-frequency transceiver devices. With the deployment of 5G mobile communication technology, microwave devices are developing toward high frequency, miniaturization and low loss. The dielectric constant for diamagnetically substituted M-type hexaferrites decreases slowly at low frequencies, and it monotonically depends on the diamagnetic substitution concentration.[49,50] The increase of the resonant frequency upon bias field increase is observed since the internal anisotropy field increases. Resonant frequency increases approximately 1.5 GHz at a bias field increase of 1 kOe. The transistor characteristics of LTOP FETs are exhibited in Fig. 5. The output current behavior of the fabricated devices is investigated by applying gate voltage from 2.5 V to 10 V in increments of 2.5 V. As can be seen, the devices exhibit low-voltage operation and an acceptable current on/off ratio ($\approx 10^4$). Figure 5a, b and c shows the I_{DS}–V_{DS} characteristic for the LTOP1, LTOP2 and LTOP3 devices, exhibiting typical square-law behavior and reaching an on current for the devices of almost 12.5, 10.0 and 8.0 nA at V_{GS} = 10 V, respectively. The operating voltage of organic-inorganic gate dielectric is decreased by increasing the organic material molar ratio of the organic-inorganic composite. This is because of the large barriers due to trap states faced by charge carriers, which increase by increasing organic material (PVP) in the gate dielectric structure. I_{DS}–V_{GS} transfer curves of the organic-inorganic TFT devices on silicon-free substrate operated at V_{DS} = 10 V are show in Fig. 5d, e and f.

The values of current on/off ($I_{on/off}$) for LTOP gate dielectric structural FETs using a ZnO channel (W/L= 20) are 1.79 × 10^4, 2.06 × 10^4 and 2.09 × 10^4 for LTOP1, LTOP2 and LTOP3 devices, respectively. The threshold voltage (V_{th}) of TFTs is extracted from a linear fit of $I_{DS}^{1/2}$ versus V_{GS}. The increase in trap state numbers at the organic gate dielectric interface leads to increased V_{th} and the large

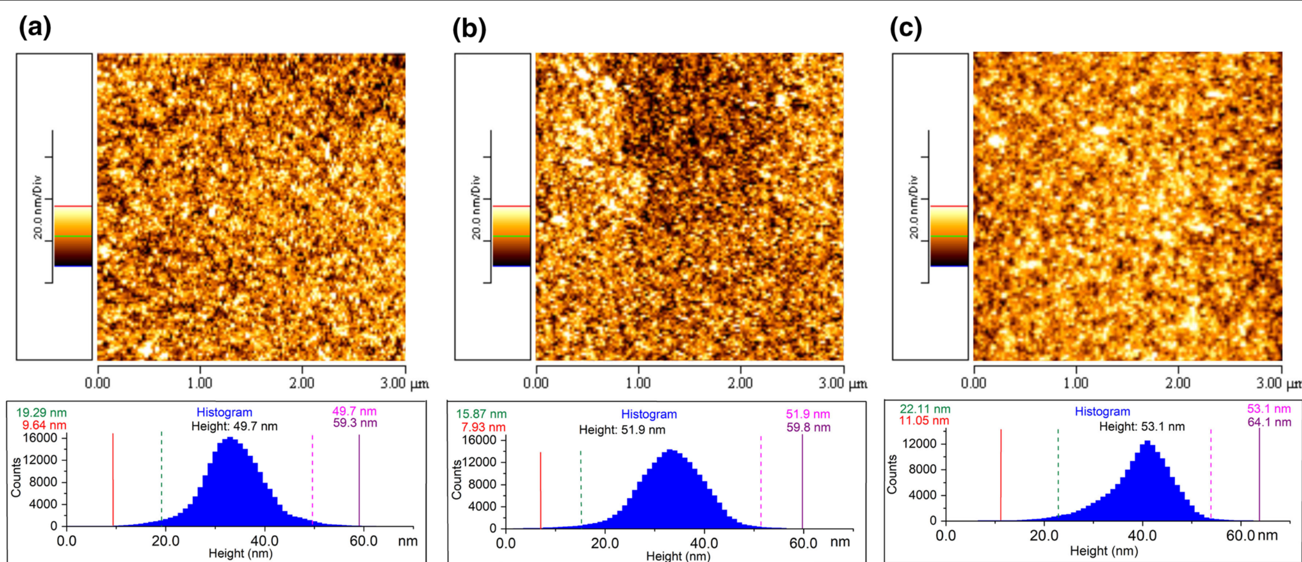

Fig. 4. The surface morphology of organic-inorganic hybrid thin films based on AFM analyze with scan size of 3 μm × 3 μm. Tapping mode AFM image with histogram curve duo to the Gaussian form with the least breadth for (a) LTOP1 sample, (b) LTOP2 sample and (c) LTOP3 sample.

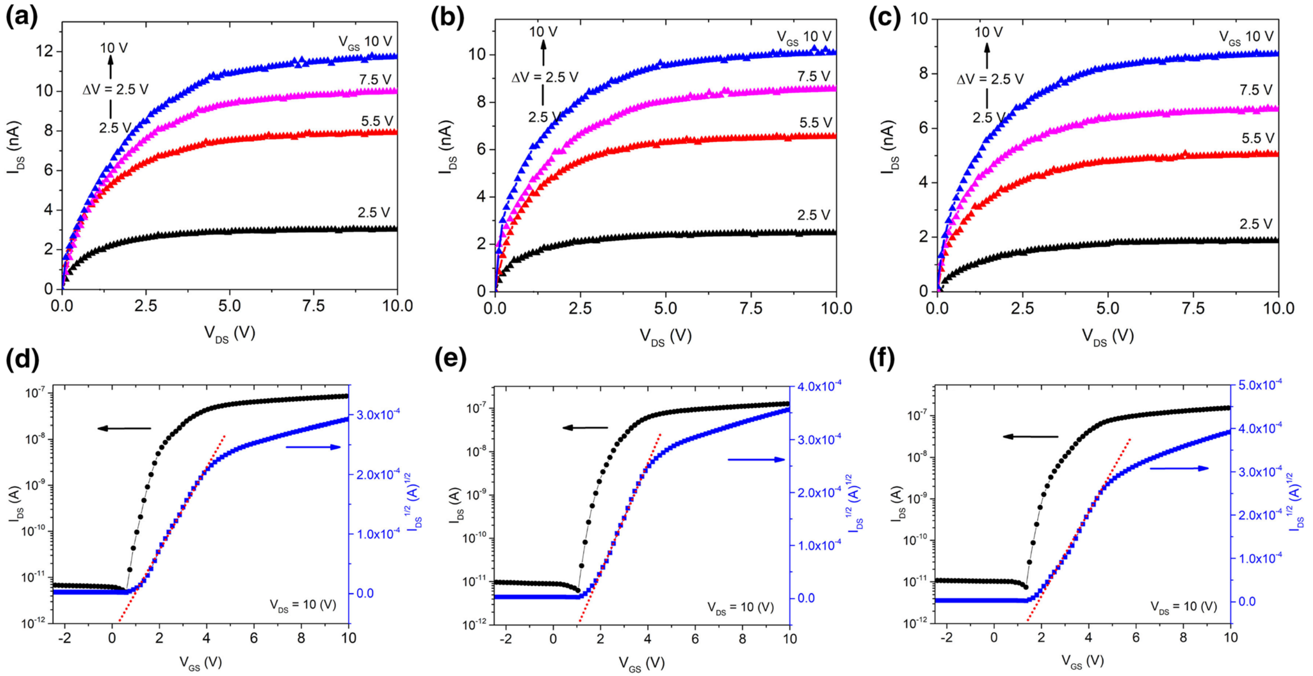

Fig. 5. Leakage current vs. voltage through the organic-inorganic composite gate dielectric of LTOP by applying gate voltages from 0 V to 10 V that raise with 2.5 V steps for (a) LTOP1 sample, (b) LTOP2 sample and (c) LTOP3 sample. The transfer characteristics of the thin film transistors based on organic-inorganic composite gate dielectric at the gate voltage equal to 10 V for (d) LTOP1 sample, (e) LTOP2 sample and (f) LTOP3 sample.

barriers due to traps faced by charge carriers. As expected, the values of V_{th} for LTOP1, LTOP2 and LTOP3 structures deduced from their correlated transfer curves increase from +0.3 to +1.0 and +1.3 V. These positive low values of V_{th} guarantee the channel current equal to zero at $V_{GS} = 0$ V by return switching without applying negative voltages.

Another important parameter for transistor characterization is the saturation field-effect mobility (μ_{sat}) that is calculated from the following equation:[51,52]

$$I_{DS,sat} = \frac{C\mu_{sat}W}{2L}(V_{GS} - V_{th})^2 \tag{1}$$

where L and W are channel length and width, respectively, and C is the capacitance per unit area of gate dielectric film. The evaluated μ_{sat} values for LTOP1, LTOP2 and LTOP3 are 1.04, 0.87 and 0.49 cm^2 $V^{-1}s^{-1}$, respectively. These values together with threshold voltage and current on/off are summarized in Table II.

Table II. Properties of the fabricated organic-inorganic composite gate dielectric.

Sample	V_{th} (V)	μ_{sat} (cm^2 $V^{-1}s^{-1}$)	$I_{(on/off)}$
LTOP1	+0.3	1.04	1.79×10^4
LTOP2	+1.0	0.87	2.06×10^4
LTOP3	+1.3	0.49	2.09×10^4

CONCLUSION

Lanthanum titanate-PVP composite was prepared successfully by a low thermal synthesis method using a solution-processable technique. In order to characterize the organic-inorganic composite, various evaluating methods were utilized, including TGA, XRD, FTIR and XPS analyses. The facile deposition technique (spin coating) was used to coat the synthesized organic-inorganic composite gate dielectric layer on PET-ITO substrate. The operation voltage of the device was estimated and reduced to 10 V. The electron mobility, threshold voltage and current on/off were 1.04 cm^2 $V^{-1}s^{-1}$, +0.3 and 1.79×10^4, respectively, for the best fabricated sample (LTOP1). Low-voltage organic-inorganic composite FETs have the potential advantage of low cost and low power consumption for portable and flexible electronics.

CONFLICT OF INTEREST

The authors declare that they have no conflict of interest.

REFERENCES

1. S. Yadav, and S. Ghosh, *ACS Appl. Mater. Inter.*, 2016, **8**, p 10436.
2. H. Najafi-Ashtiani, *Appl. Surf. Sci.*, 2018, **455**, p 373.
3. H. Chen, Y. Guo, G. Yu, Y. Zhao, J. Zhang, D. Gao, H. Liu, and Y. Liu, *Adv. Mater.*, 2012, **24**, p 4618.
4. S. Jung, M. Albariqi, G. Gruntz, T. Al-Hathal, A. Peinado, E. Garcia-Caurel, Y. Nicolas, T. Toupance, Y. Bonnassieux, and G. Horowitz, *ACS Appl. Mater. Inter.*, 2016, **8**, p 14701.

5. J. Huang, H. Zhu, Y. Chen, C. Preston, K. Rohrbach, J. Cumings, and L. Hu, *ACS Nano*, 2013, **7**, p 2106.
6. T. Rembert, C. Battaglia, A. Anders, and A. Javey, *Adv. Mater.*, 2015, **27**, p 6090.
7. I. Isakov, H. Faber, M. Grell, G. Wyatt-Moon, N. Pliatsikas, T. Kehagias, G. P. Dimitrakopulos, P. P. Patsalas, R. Li, and T. D. Anthopoulos, *Adv. Funct. Mater.* 27 (2017).
8. O. Acton, G. Ting, H. Ma, J.W. Ka, H. Yip, N.M. Tucker, and A.K.Y. Jen, *Adv. Mater.*, 2008, **20**, p 3697.
9. E.M.C. Fortunato, P.M.C. Barquinha, A.C.M.B.G. Pimentel, A.M.F. Gonçalves, A.J.S. Marques, L.M.N. Pereira, and R.F.P. Martins, *Adv. Mater.*, 2005, **17**, p 590.
10. F. Igbari, Q. Shang, Y. Xie, X. Zhang, Z. Wang, and L. Liao, *RSC Adv.*, 2016, **6**, p 28801.
11. A. Kumar, S. Mondal, and K.S.R.K. Rao, *Appl. Surf. Sci.*, 2015, **370**, p 373.
12. J. Huang, Y. Tsai, M. Tsai, L. Huang, M. Lee, and M. Chen, *Appl. Surf. Sci.*, 2015, **324**, p 662.
13. M.D. Morales-Acosta, M.A. Quevedo-López, and R. Ramírez-Bon, *Mater. Chem. Phys.*, 2014, **146**, p 380.
14. Y. Chang, M. Yu, R. Lin, C. Hsu, and T. Hou, *Appl. Phys. Lett.*, 2016, **108**, p 033502.
15. K. Satoh, Y. Yamada, Y. Kanaoka, S. Murakami, Y. Kakehi, and Y. Sakurai, *Jpn. J. Appl. Phys.*, 2019, **58**, p 038004.
16. T. Partida-Manzanera, Z.H. Zaidi, J.W. Roberts, S.B. Dolmanan, K.B. Lee, P.A. Houston, P.R. Chalker, S. Tripathy, and R.J. Potter, *J. Appl. Phys.*, 2019, **126**, p 034102.
17. K. Kandpal, N. Gupta, J. Singh, and C. Shekhar, *J. Electron. Mater.*, 2020, **49**, p 3156.
18. S.Y. Tan, *J. Electron. Mater.*, 2010, **39**, p 2435.
19. D.A. Vinnik, V.E. Zhivulin, A. Yu Starikov, S.A. Gudkova, E.A. Trofimov, A.V. Trukhanov, S.V. Trukhanov, V.A. Turchenko, V.V. Matveev, E. Lahderanta, E. Fadeev, T.I. Zubar, M.V. Zdorovets, and A.L. Kozlovsky, *J. Magn. Magn. Mater.*, 2020, **498**, p 166117.
20. A.L. Kozlovskiy, I.E. Kenzhina, and M.V. Zdorovets, *Ceram. Int.*, 2020, **46**, p 10262.
21. Y. Fujisaki, H. Koga, Y. Nakajima, M. Nakata, H. Tsuji, T. Yamamoto, T. Kurita, M. Nogi, and N. Shimidzu, *Adv. Funct. Mater.*, 2014, **24**, p 1657.
22. P.Wang, D. Zhou, H.Guo, W. Liu, J. Su, M. Fu, C. Singh, and S.A. Trukhanov, *J. Mater. Chem. A.* 8, 11124 (2020).
23. A.L. Kozlovskiy, and M.V. Zdorovets, *Compos. B. Eng.*, 2020, **191**, p 107968.
24. H. Najafi-Ashtiani, A. Bahari, S. Gholipour, and S. Hoseinzadeh, *Appl. Phys. A.*, 2018, **124**, p 1.
25. A. Liu, G. Liu, H. Zhu, B. Shin, E. Fortunato, R. Martins, and F. Shan, *Appl. Phys. Lett.*, 2016, **108**, p 233506.
26. K. Kim, G. Park, H. Fukidome, T. Suemitsu, T. Otsuji, W. Cho, and M. Suemitsu, *Jpn. J. Appl. Phys.* 56, 06GF09 (2017).
27. S.Y. Je, B.G. Son, H.G. Kim, M.Y. Park, L.M. Do, R. Choi, and J.K. Jeong, *ACS Appl. Mater. Inter.*, 2014, **6**, p 18693.
28. L.Y. Matzui, A.V. Trukhanov, O.S. Yakovenko, L.L. Vovchenko, V.V. Zagorodnii, V.V. Oliynyk, M.O. Borovoy, E.L. Trukhanova, K.A. Astapovich, D.V. Karpinsky, and S.V. Trukhanov, *Nanomaterials*, 2019, **9**, p 1720.
29. M.A. Darwish, A.V. Trukhanov, O.S. Senatov, A.T. Morchenko, S.A. Saafan, K.A. Astapovich, S.V. Trukhanov, E.L. Trukhanova, A.A. Pilyushkin, A. Sergio, B. Sombra, D. Zhou, R.B. Jotania, and C. Singh, *Nanomaterials*, 2020, **10**, p 492.
30. H. Najafi-Ashtiani, and A. Bahari, *Opt. Mater.*, 2016, **58**, p 210.
31. H. Najafi-Ashtiani, and A. Bahari, *Synth. Met.*, 2016, **217**, p 19.
32. H. Najafi-Ashtiani, A. Bahari, and S. Ghasemi, *J. Electroanal. Chem.*, 2016, **774**, p 14.
33. H. Najafi-Ashtiani, A. Bahari, and S. Ghasemi, *Org. Electron.*, 2016, **37**, p 213.
34. W. C. Shin, H. Moon, S. Yoo, Y. Li, and B. Jin Cho, *IEEE Electron Device Lett. 31, 1308* (2010).
35. H. Najafi-Ashtiani, *J. Mater. Sci. Mater.*, 2019, **30**, p 7087.
36. Y. Ha, S. Jeong, J. Wu, M. Kim, V.P. Dravid, A. Facchetti, and T.J. Marks, *J. Am. Chem. Soc.*, 2010, **132**, p 17426.
37. R.P. Ortiz, A. Facchetti, and T.J. Marks, *Chem. Rev.*, 2010, **110**, p 205.
38. S. Jeong, D. Kim, S. Lee, B. Park, and J. Moon, *Appl. Phys. Lett.*, 2006, **89**, p 264101.
39. M. Shahbazi, A. Bahari, and S. Ghasemi, *Synth. Met.*, 2016, **221**, p 332.
40. A. Hashemi, A. Bahari, and S. Ghasemi, *Appl. Surf. Sci.*, 2017, **416**, p 234.
41. S.V. Trukhanov, I.O. Troyanchuk, N.V. Pushkarev, and H. Szymczak, *J. Exp. Theor. Phys.*, 2002, **95**, p 308.
42. M.V. Zdorovets, and A.L. Kozlovskiy, *Ceram. Int.*, 2020, **46**, p 14548.
43. B.I. Edmondson, S. Liu, S. Lu, H. Wu, A. Posadas, D.J. Smith, X.P.A. Gao, A.A. Demkov, and J.G. Ekerdt, *J. Appl. Phys.*, 2018, **124**, p 185303.
44. F. J. Jing, L. Wang, Y. W. Liu, R. K. Y. Fu, X. B. Zhao, R. Shen, N. Huang, and Paul K. Chu, *Thin Solid Films.* 515, 1219 (2006).
45. C.Y. Han, W.M. Tang, and P.T. Lai, *IEEE Trans. Electron. Devices.*, 2017, **64**, p 1716.
46. Y. Baek, S. Lim, L.H. Kim, S. Park, S.W. Lee, T.H. Oh, S.H. Kim, and C.E. Park, *Org. Electron.*, 2016, **28**, p 139.
47. M.V. Zdorovets, I.E. Kenzhina, V. Kudryashov, and A.L. Kozlovskiy, *Ceram. Int.*, 2020, **46**, p 10521.
48. S.V. Trukhanov, V.A. Khomchenko, L.S. Lobanovski, M.V. Bushinsky, D.V. Karpinsky, V.V. Fedotova, I.O. Troyanchuk, A.V. Trukhanov, S.G. Stepin, R. Szymczak, C.E. Botez, and A. Adair, *J. Exp. Theor. Phys.*, 2006, **103**, p 398.
49. A.V. Trukhanov, V.G. Kostishyn, L.V. Panina, V.V. Korovushkin, V.A. Turchenko, P. Thakur, A. Thakur, Y. Yang, D.A. Vinnik, E.S. Yakovenko, L. Yu Matzui, E.L. Trukhanova, and S.V. Trukhanov, *J. Alloys Compd.*, 2018, **754**, p 247.
50. D.A. Vinnik, F.V. Podgornov, N.S. Zabeivorota, E.A. Trofimov, V.E. Zhivulin, A.S. Chernukha, M.V. Gavrilyak, S.A. Gudkova, D.A. Zherebtsov, A.V. Ryabov, S.V. Trukhanov, T.I. Zubar, L.V. Panina, S.V. Podgornaya, M.V. Zdorovets, and A.V. Trukhanov, *J. Magn. Magn. Mater*, 2020, **498**, p 166190.
51. H. Byun, E. You, and Y. Ha, *Appl. Phys. Lett.*, 2019, **114**, p 013301.
52. A. Bahari, and M. Shahbazi, *J. Electron. Mater.*, 2015, **45**, p 1201.

Publisher's Note Springer Nature remains neutral with regard to jurisdictional claims in published maps and institutional affiliations.